AD-A159 942 HELIUM SCATTERING STUDIES OF THE SURFACE STRUCTURE AND DYNAMICS OF RARE GAS CRYSTALS(U) CHICAGO UNIV IL JAMES FRANCK INST K D GIBSON ET AL. AUG 85 TR-10 1/1

UNCLASSIFIED N00014-77-C-0240 F/G 20/12 NL

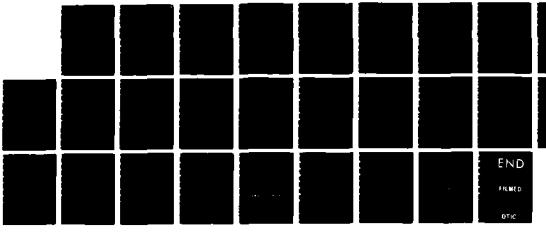

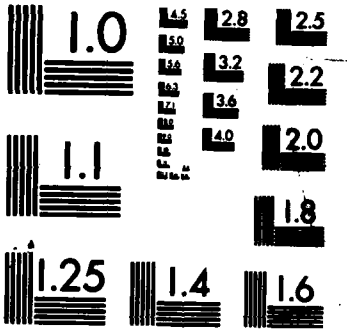

Unclassified

SECURITY CLASSIFICATION OF THIS PAGE (When Data Entered)

(2)

AD-A159 942

DTIC FILE COPY

REPORT DOCUMENTATION PAGE

READ INSTRUCTIONS BEFORE COMPLETING FORM

1. REPORT NUMBER: 10	2. GOVT ACCESSION NO.
3. RECIPIENT'S CATALOG NUMBER	
4. TITLE (and Subtitle): HELIUM SCATTERING STUDIES OF THE SURFACE STRUCTURES AND DYNAMICS OF RARE GAS CRYSTALS	5. TYPE OF REPORT & PERIOD COVERED: Interim Technical Report
6. PERFORMING ORG. REPORT NUMBER	
7. AUTHOR(s): K. D. Gibson and S. J. Sibener	8. CONTRACT OR GRANT NUMBER(s): N00014-77-C-0240
9. PERFORMING ORGANIZATION NAME AND ADDRESS: The University of Chicago, The James Franck Institute, 5460 South Ellis Avenue, Chicago, IL 60637	10. PROGRAM ELEMENT, PROJECT, TASK AREA & WORK UNIT NUMBERS: NR-392-023
11. CONTROLLING OFFICE NAME AND ADDRESS: Office of Naval Research, Physical Sciences Division (Code 421), 800 North Quincy Str., Arlington, VA 22217	12. REPORT DATE: August, 1985
	13. NUMBER OF PAGES: 32
14. MONITORING AGENCY NAME & ADDRESS(if different from Controlling Office)	15. SECURITY CLASS. (of this report): unclassified
	15a. DECLASSIFICATION/DOWNGRADING SCHEDULE

16. DISTRIBUTION STATEMENT (of this Report)

This document has been approved for public release and sale; its distribution in unlimited.

17. DISTRIBUTION STATEMENT (of the abstract entered in Block 20, if different from Report)

18. SUPPLEMENTARY NOTES

Prepared for Publication in Faraday Discussion No. 80: Physical Interactions and Energy Exchange at the Gas-Solid Interface.

19. KEY WORDS (Continue on reverse side if necessary and identify by block number) cont'd

Inelastic single phonon scattering; surface phonon dispersion relations; helium diffraction; selective adsorption; rare gas interaction potentials; thin film dynamics; gas-surface energy exchange; thin film growth; wetting; physisorption.

20. ABSTRACT (Continue on reverse side if necessary and identify by block number)

We review our experiments involving He scattering from the surfaces of ordered rare gas overlayers physisorbed on Ag(111). The series of rare gases studied were Ar, Kr, and Xe. The measurements were performed on thin film structures which were grown on a layer-by-layer basis, from monolayer to thick film, in order to study how the surface properties changed with increasing distance from the substrate. Three types of experiments are discussed; elastic diffraction, selective adsorption, and inelastic single phonon scattering by angle-resolved time-of-flight. These experiments, taken together, provide a broad overview of

DD FORM 1 JAN 73 1473 EDITION OF 1 NOV 65 IS OBSOLETE

S/N 0102-LF-014-6601

unclassified

SECURITY CLASSIFICATION OF THIS PAGE (When Data Entered)

the static and dynamic surface properties of rare gas overlayers. They also provide information about the forces which govern the adatom-adatom and adatom-substrate interactions.

A COMPLETE COPY OF THE MANUSCRIPT WILL BE SENT UPON REQUEST.

HELIUM SCATTERING STUDIES OF THE SURFACE STRUCTURE AND DYNAMICS OF RARE GAS CRYSTALS

K. D. Gibson and S. J. Sibener

The James Franck Institute and Department of Chemistry
The University of Chicago, Chicago, IL., 60637

ABSTRACT

This report
~~We~~ reviews ~~our~~ experiments involving He scattering from the surfaces of ordered rare gas overlayers physisorbed on Ag(111). The series of rare gases studied were Ar, Kr, and Xe. The measurements were performed on thin film structures which were grown on a layer-by-layer basis, from monolayer to thick film, in order to study how the surface properties changed with increasing distance from the substrate. Three types of experiments are discussed; elastic diffraction, selective adsorption, and inelastic single phonon scattering by angle-resolved time-of-flight. These experiments, taken together, provide a broad overview of the static and dynamic surface properties of rare gas overlayers. They also provide information about the forces which govern the adatom-adatom and adatom-substrate interactions.

Originator Supplied Keywords include:

See DD1473

In press Faraday Discussion No. 80: Physical Interactions and Energy Exchange at the Gas-Solid Interface.

INTRODUCTION

In recent years there has been much interest in studying rare gas overlayers physisorbed on graphite and transition metal surfaces, using H [1,2] and He [3,4] atom scattering. These relatively simple adsorption systems are of particular interest as their structural and dynamic properties can be theoretically modelled with high accuracy. This allows them to serve as excellent systems for testing ideas on adsorption and interfacial charge density distributions. These studies are based upon our extensive knowledge of the rare gas pair potentials [5], which are accurately known from gas phase measurements. Comparison between theory and experiment can therefore be used to evaluate the importance of higher order terms, such as three body forces, in the construction of the interaction potential at the surface. In addition, these highly corrugated surfaces provide good test systems for examining various approximations that are currently being used in gas-surface scattering calculations.

In this paper, we will review the results of our experiments on ordered rare gas overlayers physisorbed on a Ag(111) substrate. These studies involved both elastic and inelastic He scattering measurements, including elastic diffraction, selective adsorption, and angle-resolved time-of-flight experiments. Our investigations used Ar, Kr, and Xe as the adsorbates. The experiments were done on a layer-by-layer basis, from monolayer to thick film, to investigate how the surface properties evolved with increasing distance from the substrate.

A novel feature of this work is that we have extracted the probabilities and lineshapes for the inelastic transitions. This has resulted in the direct observation of dynamical adatom-substrate coupling. The frequency of the monolayer $SP_{\perp}$ mode overlaps those of the substrate's surface modes across part of the surface Brillouin zone (SBZ) near $\bar{\Gamma}$. In this overlap region, the linewidths of the inelastic transitions are significantly broader than near $\bar{M}$, where the substrate's surface modes have a higher frequency. This is a clear example of radiative damping by coupling between the adatom vibrations and those of the substrate. The inelastic scattering probabilities of this mode are enhanced where the frequency crosses the Ag Rayleigh mode, which is sagittally polarized. This can be explained by a direct resonance between the adatom vibrations and this substrate mode.

EXPERIMENTAL

The substrate for these experiments was a single crystal of Ag, cut and polished within 0.5° of the (111) face, as verified by Laue X-ray back reflection. Surface cleanliness was checked using Auger spectroscopy. This was done on a daily basis, as it was found that a small amount of contamination could cause major changes in the structures of the rare gas overlayers. For example, it was observed that 1% Cl coverage caused a mosaic in the monolayers, with parts of the surface having structures that were rotated by 30° from the expected orientation. When necessary, the Ag crystal was cleaned by Ar^+ bombardment, followed by annealing at 750 K. Surface

coherence was checked by analyzing the specular reflection angular profile of a 63 meV He beam, and was found to be $\approx$100 Å. The Ag crystal's azimuthal orientation was checked with H_2 diffraction. Crystal temperature was monitored by a Chromel-Alumel thermocouple welded directly to the back of the sample. Cooling for these experiments was done with liquid He, with a temperature stability of better than 1 K. The temperature calibration of the crystal was probably accurate to within 2 K. The lowest temperature we could achieve was 21 K.

The crystal manipulator had independent adjustments for the incident polar and azimuthal angles. Once the crystal azimuthal angle was determined by observing diffraction along a high symmetry direction, a circular ruled scale attached to the crystal mount was used to confirm the azimuth setting for angles falling between high symmetry directions. The crystal was welded to platinum support rods attached to the manipulator, and rapid heating was done resistively with a voltage-programmable power supply, its output adjusted by a controller using feedback from the thermocouple on the crystal.

Detection was done with a doubly-differentially ion pumped quadrupole mass spectrometer (crystal to ionizer distance of 14.45 cm.). The actual detection was done with a venetian blind electron multiplier, suitable for doing pulse counting. The machine is designed so that the incident angle, Θ_i, and the scattering angle probed are are independently variable. A more complete description of the scattering chamber is given elsewhere [6]. Data collection was done with a PDP-11/20 minicomputer, which was interfaced to the data taking electronics via CAMAC.

The He probe beam was generated by supersonic expansion through a 12.5 μ orifice. Two distinct beam energies were used in the experiments reported: 66 meV ($\Delta v/v \approx 2.5\%$) and 18 meV ($\Delta v/v \approx 1.1\%$). The latter was produced by cooling the source with liquid N_2. After being skimmed, the beam was chopped by a rotating slotted disk, and collimated to a 0.3° angular spread before entering the scattering chamber.

All of the rare gases form azimuthally aligned, but translationally incommensurate structures with the Ag(111) surface. Structural and thermodynamic information for the rare gas overlayers was already available from the work of Unguris et. al. [7]. With the phase diagrams from these papers, we first formulated a method for growing ordered and reproducible monolayers. Dosing was done with a low pressure side beam, inclined at 15° to the scattering plane. This beam could be flagged on and off within a few milliseconds by means of a computer-controlled shutter before entering the scattering chamber. The rare gas pressure at the crystal surface was $\approx 10^{-7}$ torr when the shutter was open, and the beam spot diameter was $\approx$2.5 mm., twice that of the He beam.

To grow the Xe monolayer, the crystal was dosed at $\Theta_i = 0°$ for 1 min. at a surface temperature, T_s, of 75 K. Then, with the dosing beam still on, the surface temperature was dropped to $\approx$57 K. At this point, the dosing beam was stopped, and the crystal rotated to $\Theta_i = 70°$. The crystal was then dosed for another minute at $T_s = 57$ K. The surface temperature was then dropped to 25 K. Finally, the crystal was reheated to $T_s \approx 57$ K for at least 5 min. to anneal the Xe monolayer. Kr monolayers were grown similarly, except that the first

dose was at T_s=57 K, and the surface temperature of the second dose and anneal was 42 K. Ar monolayers were grown by first dosing at T_s=44 K for 1 minute, Θ_i=70° . With the dosing beam still on, the surface temperature was then dropped to ≈28 K. Just as this temperature was reached, the dosing beam was flagged off. This monolayer was annealed for at least 10 min. at T_s=28 K.

It was imperative that a good monolayer be grown before any attempt was made at multilayer growth. Multilayers were grown on a layer-by-layer basis using dosing times. Between the deposition of each successive layer, there was a short anneal time near the desorption temperature. When the experiments on a particular overlayer were completed, coverage was checked using Temperature Programmed Thermal Desorption (TPD). The influence of the Ag-rare gas potential was such that 1, 2, and 3 layers desorb at progressively lower temperatures. The TPD peak due to the monolayer was distinct from those of the other overlayers, and so by comparing the total integrated area to that of the monolayer, a quantative measure of the coverage could be obtained. Only data collected on films typically falling within 5% of a particular overlayer were used for 1, 2, and 3 layers. The deviation from an integral number of layers was much greater for the≥ 25 layer results.

The He beam was used to check the quality of the overlayers by comparing the intensity ratio of the specular reflection to those of the higher order diffraction peaks. These ratios typically did not vary by more than 10% from one film to the next for a particular overlayer.

RESULTS AND DISCUSSION

Figure 1 shows typical diffraction spectra for an 18 meV He scattering from 1, 2, 3, and 25 layer films. The expected in-plane diffraction peaks are clearly seen, indicating the high quality of our grating. By deconvoluting the width of the instrument function from that of the experimental results, an estimate of the coherence length of the overlayers can be made using simple perturbation theory [8], assuming only finite size effects. This coherence length is $\approx$100 Å, and is only slightly smaller than that of the Ag substrate. A further indication of the quality of the overlayers is the very low diffuse background. Though this does not prove that we are observing strictly layer-by-layer growth (Type 1 [9]), it does indicate that the overlayers are wetting sufficiently so as not to be roughened. The positions of the diffraction peaks were used to determine the lattice constants, given in Table 1. For the multilayers, these values are very close to the corresponding bulk values determined by X-ray diffraction [10]. The monolayer value is slightly larger than the overlayer values for all of the systems we have examined. The monolayer values given are actually a time average, as these structures slowly shrank by as much as 0.04 Å. After several hours, the values had still not reached the bulk values, and did not appear to be compressing further. However, we did not follow any monolayer for more than 5 or 6 hours.

In principle, comparison between close-coupled scattering calculations and elastic scattering data can be used to extract the He-surface potential. Our experience is that this is more easily done using selective adsorption experiments. Once the potential has been derived,

the diffraction experiments can be used to test various simplifying approximations used for treating gas-surface scattering. Such calculations are now in progress.

Figure 2 shows scans of the specular intensity for a Xe monolayer using a 66 meV He beam (a), and an 18 meV beam (b), taken at 0.2° increments of polar angle. For this system, we have done these selective adsorption experiments at 2° increments of azimuthal angle over a 30° arc from the $<11\bar{2}>$ direction for the low energy beam, and over a 22° arc for the higher energy beam. In the free atom approximation, selective adsorption resonances occur at $\vec{k}_i^2 - 2ME_n/\hbar^2 = (\vec{K}_i + \vec{G})^2$ [11], where E_n is an energy level of the laterally averaged potential. When plotted in the $\vec{K}_x$–$\vec{K}_y$ plane, they form circles centered at $-\vec{G}$. Figure 3 is such a plot for the maxima in the 18 meV He experiments. The arcs drawn on the plot are labelled by the coupling $\vec{G}$-vector, and represent three energy levels, 4.95, 2.15, and 0.64 meV. These energies are <u>not</u> our definitive values, but only represent a possibility based upon the good fit for the maxima using the free atom approximation (final results will be based upon a comparison of the selective adsorption spectra and scattering calculations). However, it is interesting to note that for one of their model potentials, Chung et. al. [12] calculated levels of 4.98, 2.06, 0.76, and 0.23 meV for the Xe/Ag system. Their model included the He-rare gas pair potential, the long range He-Ag attraction, and three body terms. For the maxima, there are no arcs that correspond to a level near 0.23 meV, but this transition is expected to be weak. When minima were plotted in the $\vec{K}_x$–$\vec{K}_y$ plane, no set of arcs correlated as well with the data. However, with a highly corrugated system, there

is strong coupling between higher order Fourier components of the potential. This causes the resonances to be perturbed from circles where levels cross. And, since the background level is not known, it is not apparent which of the features are truly resonances, and which are merely topological (i. e. 2 "maxima" will have a "minimum" between them, or vice versa). Simple rules, such as those of Wolfe and Weare [13], predict that most of the resonances should be minima. These levels roughly agree with the minima in the spectra taken with the higher energy beam. Here, the assignment is somewhat less ambiguous, as most of the sharp features are minima. The broad undulation can be qualitatively ascribed to Bragg-like interference due to the surface corrugation. Maxima will occur at $2d\cos(\Theta)=n$, where d, the size of the corrugation, is $\approx$1.2 Å for the $<11\bar{2}>$ direction.

The only way to properly analyze this data is to compare the results with close-coupled calculations, such as those of Hutson and Schwarz for the Xe-graphite system [14]. Such an analysis not only gives the levels of the laterally averaged potential, but also the magnitude of the periodic components of the potential. This analysis is currently underway. We have selective adsorption data for all of the overlayers, along at least one azimuthal angle. Hopefully, these quantum scattering calculations will allow us to determine the He-surface potential for these systems.

To study the dynamical properties of the rare gas overlayers, we used the angle resolved time-of-flight (TOF) of inelastically scattered 18 meV He. Figure 4 shows typical TOF spectra for 1, 2, 3, and 25 layer Xe. The arrows indicate the position of the elastic time-of-

flight. We attribute the elastic component to crytal defects and incoherent scattering from these "soft" surfaces. For the multilayers, the narrow well-defined peaks are indicative of single phonon interactions. Data analysis consisted of fitting the TOF spectra with a non-linear least-squares routine. From the peak positions, and the incident and final angles, phonon momentum and energy could be determined using the conservation of energy and crystal momentum. Figure 5 shows the phonon dispersion curves for the principal modes observed, i. e. those corresponding to inelastic TOF peaks immediately adjacent to either side of the elastic TOF. The layer-by-layer evolution of the surface dynamics is clearly shown.

The monolayer $SP_\perp$ mode , the only monolayer mode we observed, is dispersionless within our experimental error. This indicates that the rare gas atoms are behaving as independent Einstein oscillators, vibrating in an uncorrelated manner in the holding potential of the Ag substrate. This behavior is consistent with previous reports dealing with rare gas monolayers physisorbed on graphite [15] and other metal surfaces [4]. The energies give the curvature of this potential at its minimum. These energies are 2.79 meV for Xe, 2.93 meV for Kr, and 3.67 meV for Ar. Using this information, the well depth [16], and the theoretical C_3 constant [17], an exponential-3 parameterization of the holding potential can be derived. This is of the form $V(z)=Aexp(-\beta(z-z_o))-C_3/(z-z_o)^3$, where z_o is the position of the reference plane. The parameters are given in Table 2. The parameters are not valid for small z, as no saturation term has been included. This analysis shows the usefulness of inelastic He scattering for determining the physisorption potentials of these heavy rare gas adatoms,

which would be difficult or impossible to obtain using selective adsorption techniques.

Figure 6 shows the energies of all the inelastic transitions for the Kr monolayer. The higher energy transitions occurred at 2 and 3 times the energy of the inelastic transitions plotted on the lowest curve in the figure. Since the mode is dispersionless, multiphonon interactions, as well as overtones, will result in discrete peaks, rather than a broad background. Near their minima, the exponential-3 potentials are nearly harmonic, so this does not allow us to differentiate between the two processes. With the help of temperature dependent data, and simple scattering calculations, we intend to address this question.

As further layers are added, the observed modes begin to disperse. At 25 layers, a bulk-like Rayleigh wave emerges. The observations for this mode could not be extended below $\approx 0.25\ Q/Q_{max}$ because the peak merged with the incoherent elastic peak. The convergence of the energies is much faster at $\overline{M}$ than at $\overline{\Gamma}$ because the displacements of the adatoms can extend several layers beneath the surface near the center of the SBZ [18]. Not all of the data in Figures 5 and 6 are for normal processes. Due to the high corrugation of these systems, Umklapp processes were quite strong. All possible combinations of $\Delta\vec{Q}$ and ΔE were observed.

Lattice dynamics and molecular dynamics calculations have been carried out [19,20,21] which quantitatively reproduce the observed vibrational frequencies of the overlayers. These calculations used realistic gas phase pair potentials for the rare gas-rare gas interaction, and a Ag holding potential derived from the monolayer vibrational

frequency, as previously described. The agreement between theory and experiment is further evidence that we are really growing our overlayers in a layer-by-layer fashion.

We are now in the process of determining the inelastic single phonon transition probabilities and linewidths. These were derived by comparing the experimental spectra with a forward convolution of the instrument response function and the phonon dispersion curves, giving the inelastic transitions a finite Lorentzian energy width. This allows us to closely reproduce the experimentally observed spectra, as shown in Figure 7. Figure 8 shows scattering probabilities, for the Kr monolayer, of the lowest energy transitions corresponding to phonon creation in the first SBZ, with $\Delta\vec{Q}<0$ (with respect to the beam). The results shown are all for $\Theta_i=45°$. This allows the probabilities taken across the SBZ to be directly compared to each other, without having to make corrections associated with selective adsorption resonances. The results as shown have not been corrected by the Debye-Waller factor, but since the energies of the transitions are not a function of $\vec{Q}$, and the final scattering angles were near 45°, the overall profile will not qualitatively change. The small change in transition probability as a function of $\vec{Q}$ seen in Figure 8 differs from the large exponential fall-off found on metals [22], and is partly due to the larger "cut-off factor", Q_c [23], for this system [24]. Note also that the probabilities peak near the position in reciprocal space where the energy of the adsorbate's Einstein mode is coincident with that of the Rayleigh mode of the Ag substrate, which is sagittally polarized. We attribute this to a resonance between the adatom vibrations and the substrate mode [25].

Linewidths are particularly interesting, as they are related to phonon lifetimes, and give information about the decay pathways for the surface vibrations. Xe monolayer linewidths are shown in Figure 9 for the lowest energy transitions corresponding to phonon creation. It is apparent that the linewidths do vary with position in the SBZ. Near $\bar{\Gamma}$, where the frequency of the Xe Einstein mode overlaps those of the Ag substrate's surface vibrational modes, the linewidths are about 1 meV. Near $\bar{M}$, where the substrate's surface modes have a much higher energy than the Xe Einstein mode, the linewidths are $\leq$0.25 meV. The same trend holds for Ar and Kr. This type of broadening is due to radiative damping by coupling with the substrate's surface modes, and has been predicted by Hall et. al. [26]. These results demonstrate that He scattering can be used to investigate how energy is transferred from the monolayer into the substrate.

The important point we wish to emphasize is that inelastic transition probabilities and lineshapes are beginning to reveal how the <u>dynamical</u> properties of ordered overlayers are influenced and modified by the <u>dynamical</u> properties of the underlying substrate. When these measurements are performed across the entire SBZ, i. e. using $\vec{Q}$ as a variable in the experiments, a wide variety of interactions and energy flow pathways can be selectively investigated.

CONCLUSION

We have reviewed the current state of our studies involving ordered rare gases physisorbed on a Ag(111) substrate. Three types of measurements aimed at examining He-surface, adatom-adatom,

and adatom-substrate interactions were discussed, including elastic diffraction, selective adsorption, and inelastic single phonon scattering. These experiments examined in particular how the surface properties of these systems evolved on a layer-by-layer basis, from monolayer to thick film. Surface phonon dispersion relations for ordered monolayer, bilayer, trilayer, and 25 layer films of Ar, Kr, and Xe physisorbed on Ag(111) were presented across the entire SBZ in the $\bar{\Gamma}$-$\bar{M}$ direction. Furthermore, examination of single phonon scattering transition probabilities and lineshapes has revealed how the dynamical properties of ordered overlayers are influenced by the dynamical properties of the underlying substrate. A detailed analysis of our experimental results, including quantum scattering calculations, is currently in progress and will be reported elsewhere.

ACKNOWLEDGEMENTS

We would like to thank C. F. Yu and D. Padowitz for experimental assistance, C. Cerjan, E. Pontius, and J. C. Light for theoretical assistance with the elastic scattering results, and B. M. Hall, D. L. Mills, and J. E. Black for theoretical collaboration involving the inelastic scattering results. This work was supported, in part, by the ONR and the NSF-MRL at the University of Chicago. S. J. Sibener also acknowledges support from a Camille and Henry Dreyfus Foundation Young Faculty Grant, an I.B.M. Faculty Development Award, and is an Alfred P. Sloan Fellow.

REFERENCES

[1] T. H. Ellis, S. Iannotta, G. Scoles, and U. Valbusa, Phys. Rev. B(24), 2307 (1981).

[2] T. H. Ellis, G. Scoles, and U. Valbusa, Surf. Sci. 118. L251 (1982).

[3] G. Bracco, P. Cantini, A. Glachant, and R. Tatarek, Surf. Sci. 125. L81 (1983).

[4] B. F. Mason and B. R. Williams, Surf. Sci. 111. 609 (1981).

[5] J. A. Barker, R. A. Fisher, and R. O. Watts, Molecular Phys. 21. 219 (1982); J. A. Barker, M. L. Klein, and M. V. Bobetic, IBM J. Res. Develop. 20. 222 (1976).

[6] C. A. Becker, Ph. D. Thesis, University of Chicago, 1980.

[7] J. Unguris, L. W. Bruch, E. R. Moog, and M. B. Webb, Surf. Sci. 87. 415 (1979); J. Unguris, L. W. Bruch, E. R. Moog, and M. B. Webb, Surf. Sci. 109. 522 (1981).

[8] J. M. Ziman,"Principles of the Theory of Solids" (Cambridge Univ. Press, Cambridge, 1972), p. 56.

[9] J. A. Venables, G. D. T. Spiller, and M. Hanbüchen, Rep. Prog. Phys. 47. 399 (1984).

[10] P. Korpiun and E. Lüscher in "Rare Gas Solids", Vol. 2, M. L. Klein and J. A. Venables ed. (Academic Press, London, 1977) Chap. 12.

[11] H. Chow and E. D. Thompson, Surf. Sci. 59, 225 (1976).

[12] Suckmin Chung, Neal Holter, and Milton B. Cole, to be published.

[13] Karen L. Wolfe and John H. Weare, Phys. Rev. Lett. 41, 1663 (1979).

[14] Jeremy M. Hutson and Carey Schwartz, J. Chem. Phys. 79, 5179 (1983).

[15] T. H. Ellis, G. Scoles, and U. Valbusa, Chem. Phys. Lett. 94, 247 (1983).

[16] L. W. Bruch, Surf. Sci. 125, 194 (1983).

[17] E. Zaremba and W. Kohn, Phys. Rev. B(13), 2270 (1976).

[18] H. Ibach and D. L. Mills, "Electron Energy Loss Spectroscopy and Surface Vibrations" (Academic Press, New York, 1982).

[19] K. D. Gibson, S. J. Sibener, Burl. M. Hall, D. L. Mills, and J. E. Black, to be published.

[20] Gianni G. Cardini, Seamus F. O'Shea, Maurizio Marchese, and M. L. Klein, to be published.

[21] L. W. Bruch, private communication.

[22] V. Celli, G. Benedek, U. Harten, J. P. Toennies, R. B. Doak, and V. Bortolani, Surf. Sci. 143, 1376 (1984).

[23] V. Bortolani, A. Franchini, F. Nizzoli, G. Santoro, G. Benedek, and V. Celli, Surf. Sci. 128, 249 (1983).

[24] K. D. Gibson and S. J. Sibener, to be published.

[25] H. Taub, K. Carneiro, J. K. Kjems, L. Passel, and J. P. McTague, Phys. Rev. B(16), 4551 (1977).

[26] Burl M. Hall, D. L. Mills, and J. E. Black, to be published.

TABLE CAPTIONS

Table 1 Experimental values of the lattice constants, in Å, for Ar, Kr, and Xe physisorbed on Ag(111).

Table 2 Parameters for the exponential-3 rare gas-Ag holding potentials (see text).

TABLE 1

Adsorbate	Monolayer	Bilayer	Trilayer	Bulk
Ar	3.80	3.77	3.77	3.77
Kr	4.02	4.00	4.00	4.00
Xe	4.38	4.33	4.33	4.33

TABLE 2

Adsorbate	A (meV)	β ($\AA^{-1}$)	D (meV) [16]	C_3 (meV-$\AA^3$) [17]
Ar	18806	2.446	66	1623
Kr	21556	2.407	108	2263
Xe	31724	2.443	172	3277

FIGURE CAPTIONS

Figure 1 Diffraction spectra for Xe overlayers physisorbed on Ag(111), taken in the $<11\bar{2}>$ direction; with Θ_i=45°, T_s= 25 K, and an 18 meV He beam. The spectrum labelled "bulk" is for 25 layers. Conditions for all of the spectra are similar, so intensities are comparable.

Figure 2 Scans of the specular intensity for a Xe monolayer as a function of polar angle, with a He beam energy of 66 meV (a) and 18 meV (b). Both selective adsorption spectra were taken in the $<11\bar{2}>$ direction with T_s=25 K.

Figure 3 $\vec{K}_x$-$\vec{K}_y$ plot of the specular intensity maxima which occurred in the selective adsorption experiments for the Xe monolayer, using an 18 meV He beam. The specular intensity was monitored at 0.2° increments of polar angle for a fixed crystal azimuth, from approximately 25° to 75°. This was repeated for every 2° of azimuth from the $<11\bar{2}>$ to the $<01\bar{1}>$ directions. Arcs are drawn for three energy levels, assuming the free atom approximation, and are labelled with the coupling $\vec{G}$-vector (see text).

Figure 4 TOF spectra of Xe overlayers physisorbed on Ag(111); E_i= 18 meV, Θ_i=45°, and T_s=25 K. Crosses are the experimental data, and the solid lines are a least-squares fit.

Figure 5 Reduced and folded zone plots of the dispersion curves of the Ar (a), Kr (b), and Xe (c) overlayers from $\bar{\Gamma}$–$\bar{M}$. Open figures are for energy loss of the beam, closed figures are for energy gain. Representative error bars are shown for energy and momentum loss features (gain and loss are with respect to the incident beam), which occurred in the first zone (normal processes). Solid lines are polynomial fits to the data. The overlayer curves labelled bulk are for the most part 25 layers. However, for Xe, some of the points are $\approx$100 layers, and for Ar, many of the points are for $\approx$40 layers.

Figure 6 Dispersion curves for Kr monolayer, showing the three observed frequencies. Open and closed symbols are the same as for figure 5.

Figure 7 Time-of-flight spectra for 18 meV He scattering from a Xe monolayer; Θ_i=45°, Θ_f=47.9°, and T_s=25 K. The arrow indicates the position of the elastic channel. Crosses are the experimental data, and the solid line is a forward convolution of the instrument function with the phonon dispersion curve, where the transitions are given a Lorentzian energy width.

Figure 8 Inelastic transition probabilities of 18 meV He scattering from a 25 K Kr monolayer, Θ_i=45°. Data are for momentum loss (with respect to the beam), in the first SBZ, of the lowest energy transition corresponding to phonon creation. This is the largest feature in Figure 7.

Figure 9 The widths of the inelastic transitions for 18 meV He scattering from a 25 K Xe monolayer, Θ_i=45°. Data are for the lowest energy transition corresponding to phonon creation.

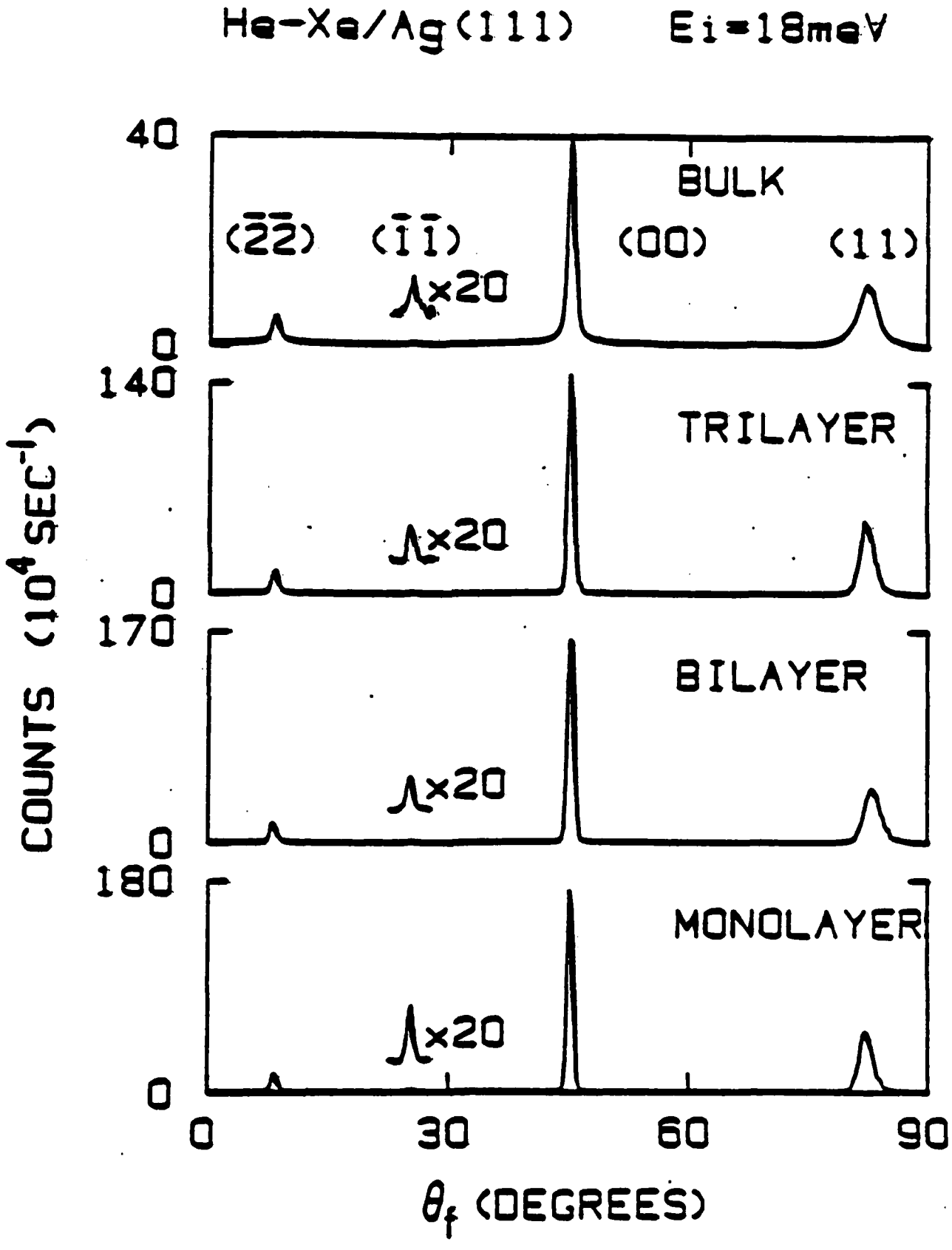
He-Xe/Ag(111) Ei=18meV
40
0
140
0
170
0
180
0
BULK
(2̄2̄) (1̄1̄)
(00) (11)
Λx20
TRILAYER
Λx20
BILAYER
Λx20
MONOLAYER
Λx20
COUNTS (10^4 SEC^-1)
0
30
60
90
θf (DEGREES)

FIGURE 1

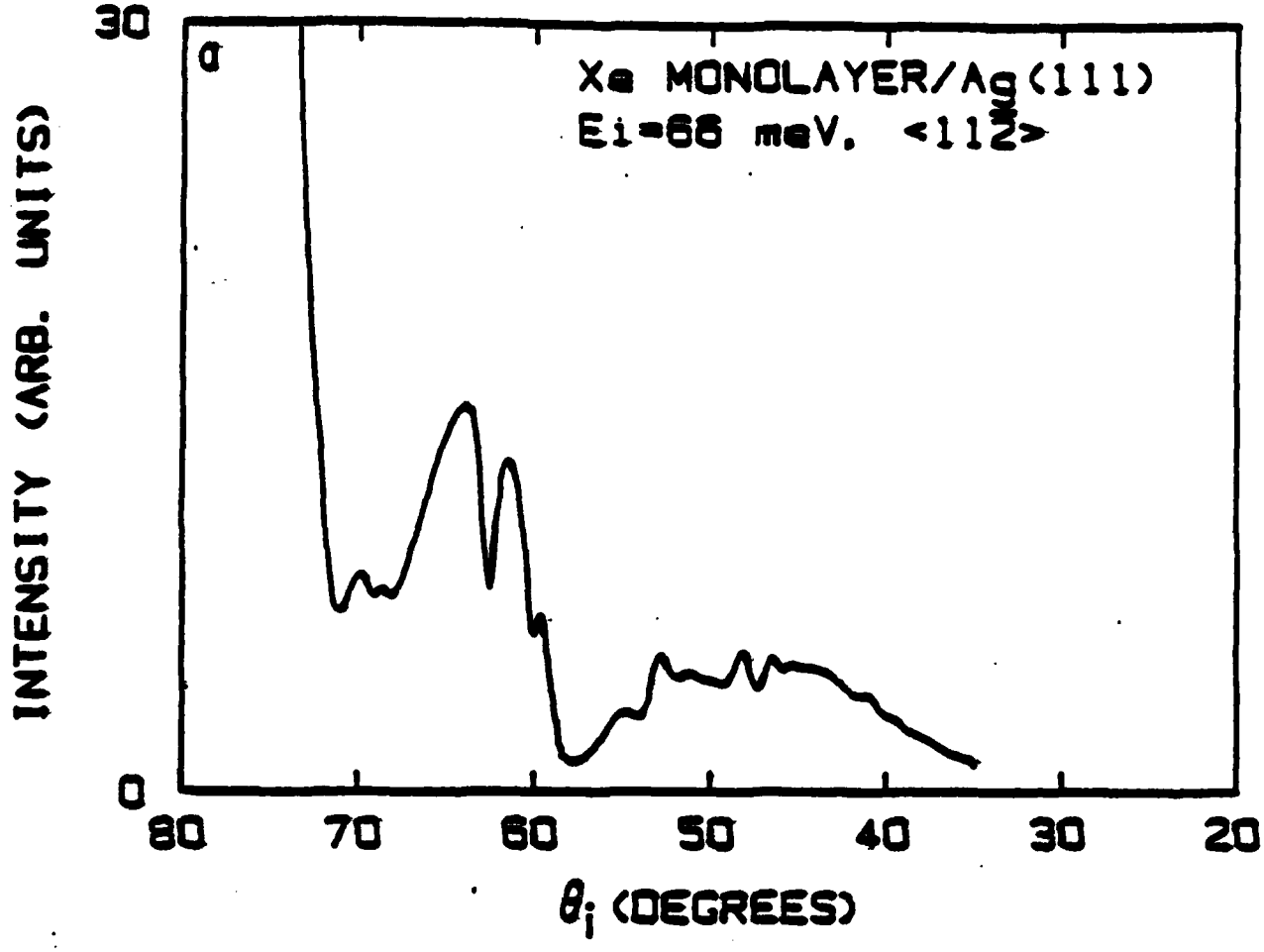
a
Xe MONOLAYER/Ag(111)
Ei=66 meV. <112>
INTENSITY (ARB. UNITS)
30
0
80
70
60
50
40
30
20
θi (DEGREES)

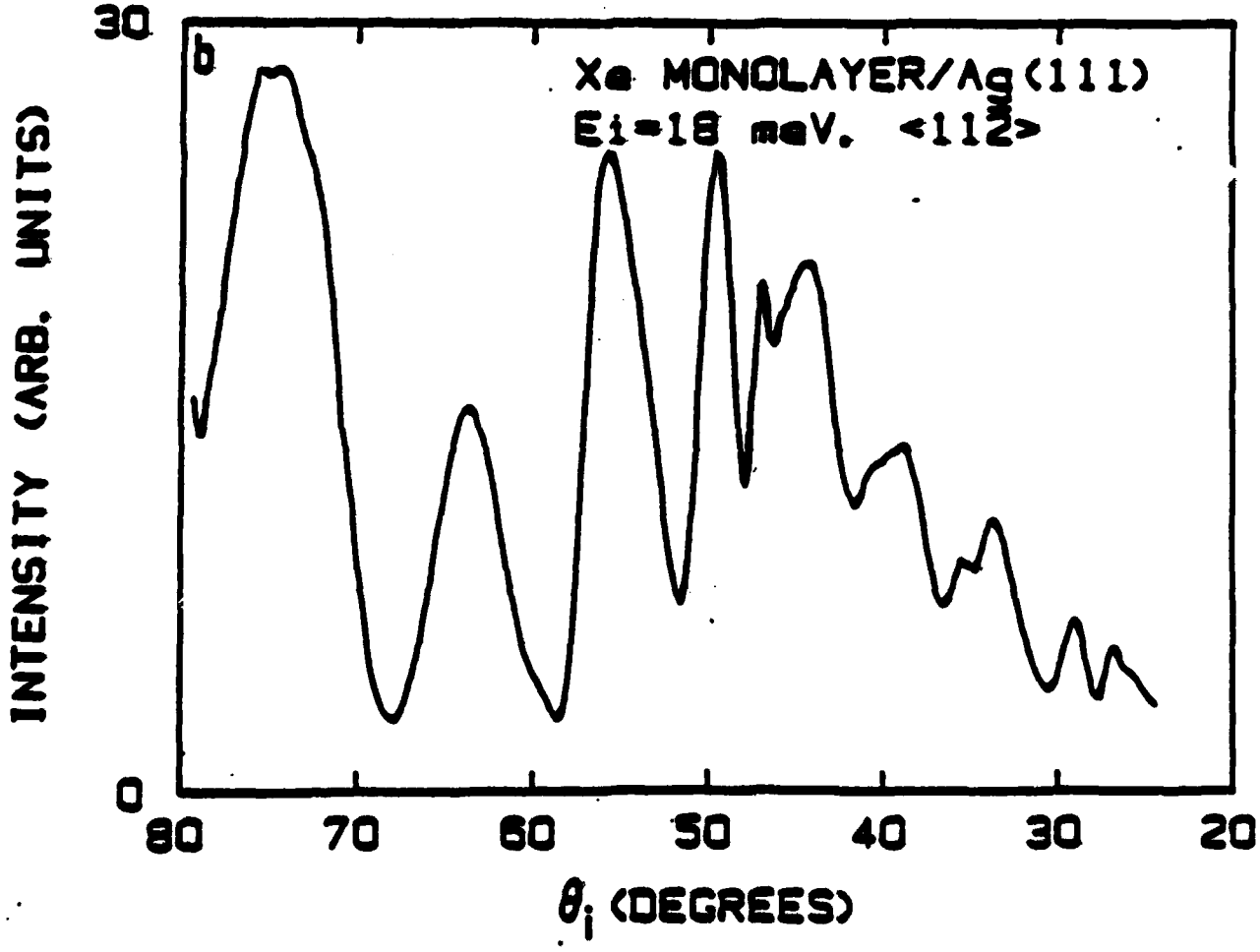
b
Xe MONOLAYER/Ag(111)
Ei=18 meV. <112>
INTENSITY (ARB. UNITS)
30
0
80
70
60
50
40
30
20
θi (DEGREES)

FIGURE 2

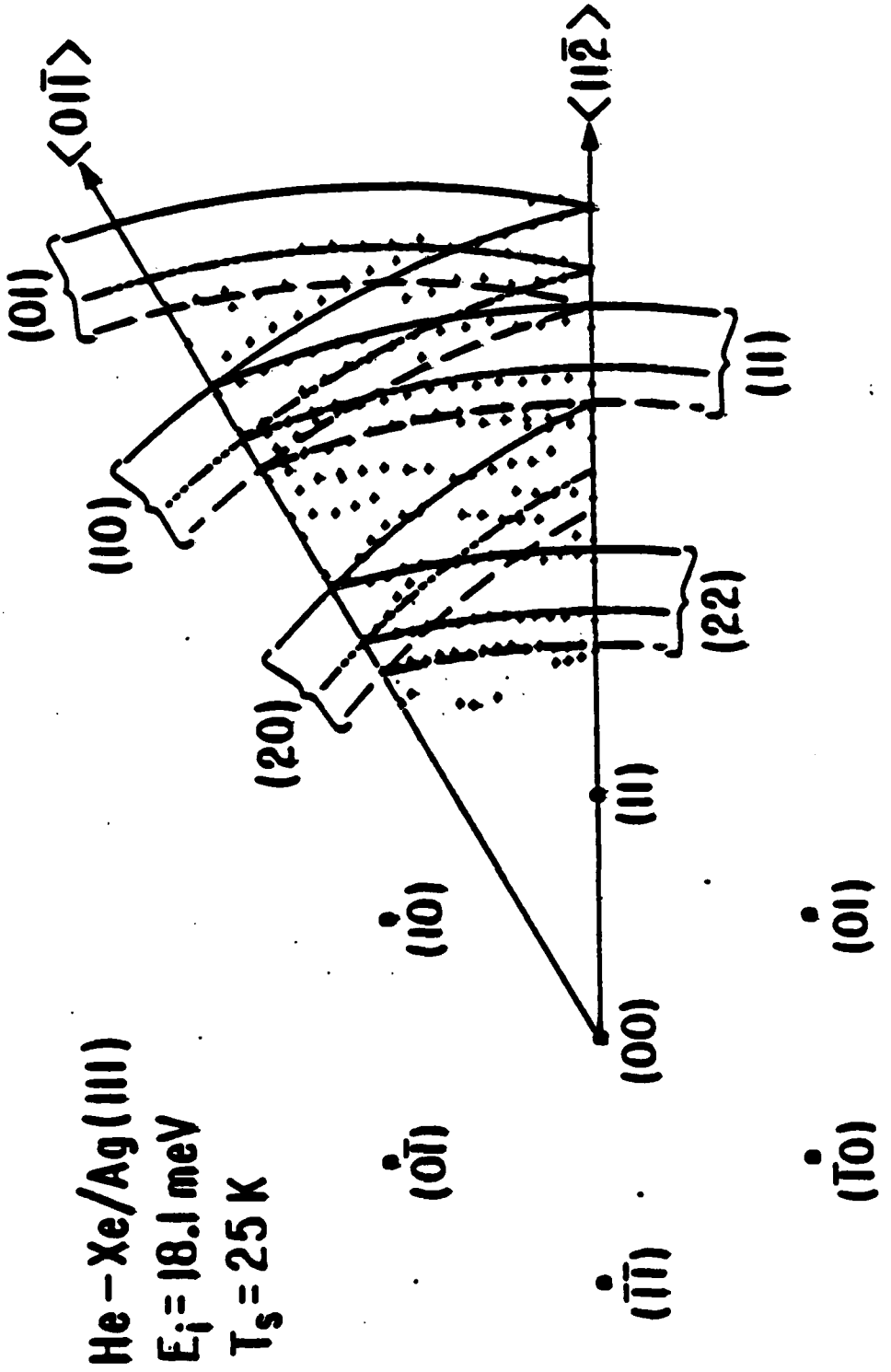
He−Xe/Ag(111)
E_i= 18.1 meV
T_s= 25 K
(00)
(10)
(01)
(11)
(20)
(22)
(11)
(01)
(10)
(11)
(01)
(10)
$\langle 01\bar{1}\rangle$
$\langle 11\bar{2}\rangle$

FIGURE 3

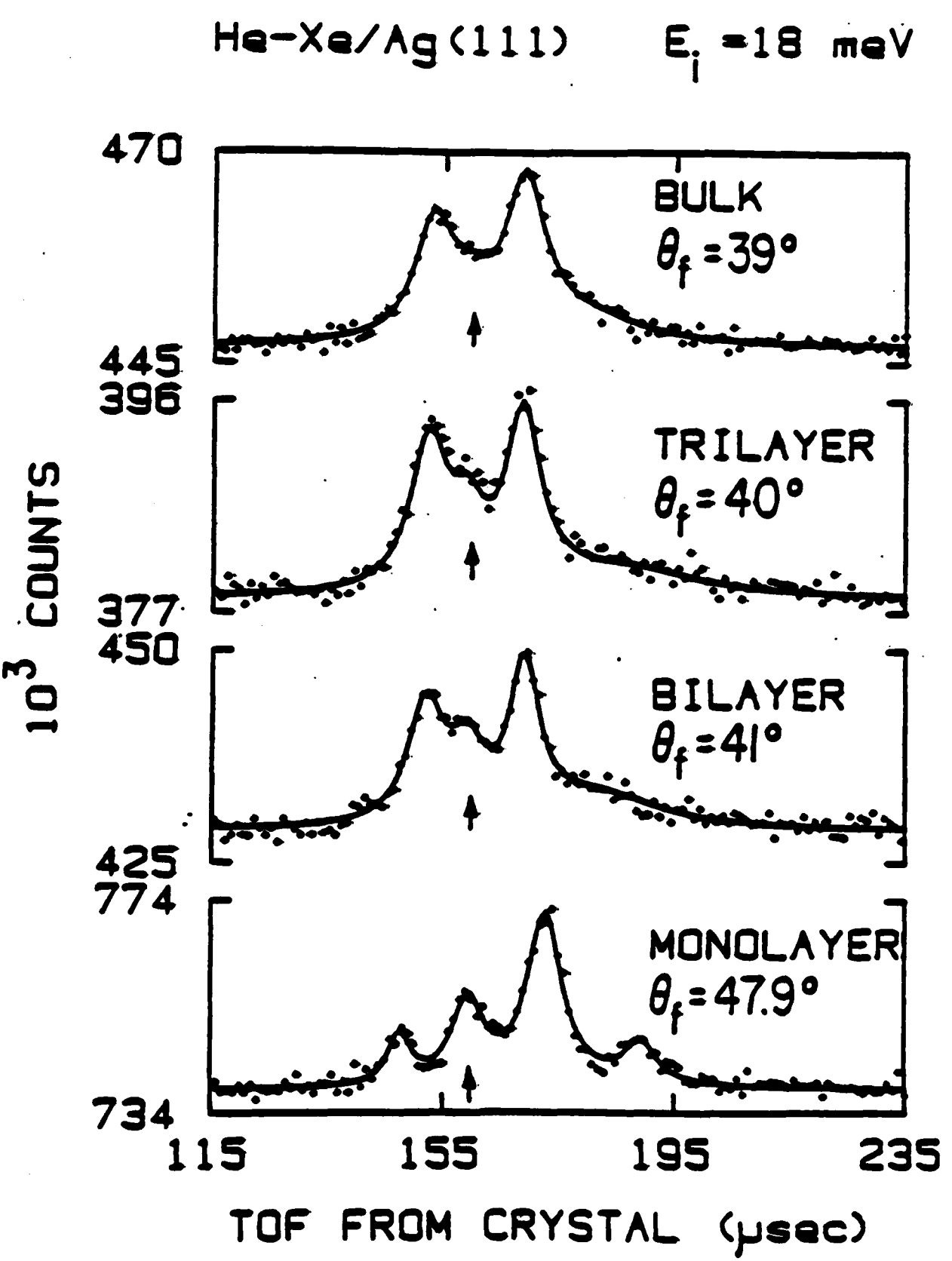
He-Xe/Ag(111) E_i =18 meV
470
445
BULK
θ_f =39°
396
377
TRILAYER
θ_f =40°
450
425
BILAYER
θ_f =41°
774
734
MONOLAYER
θ_f =47.9°
10^3 COUNTS
115
155
195
235
TOF FROM CRYSTAL (μsec)

FIGURE 4

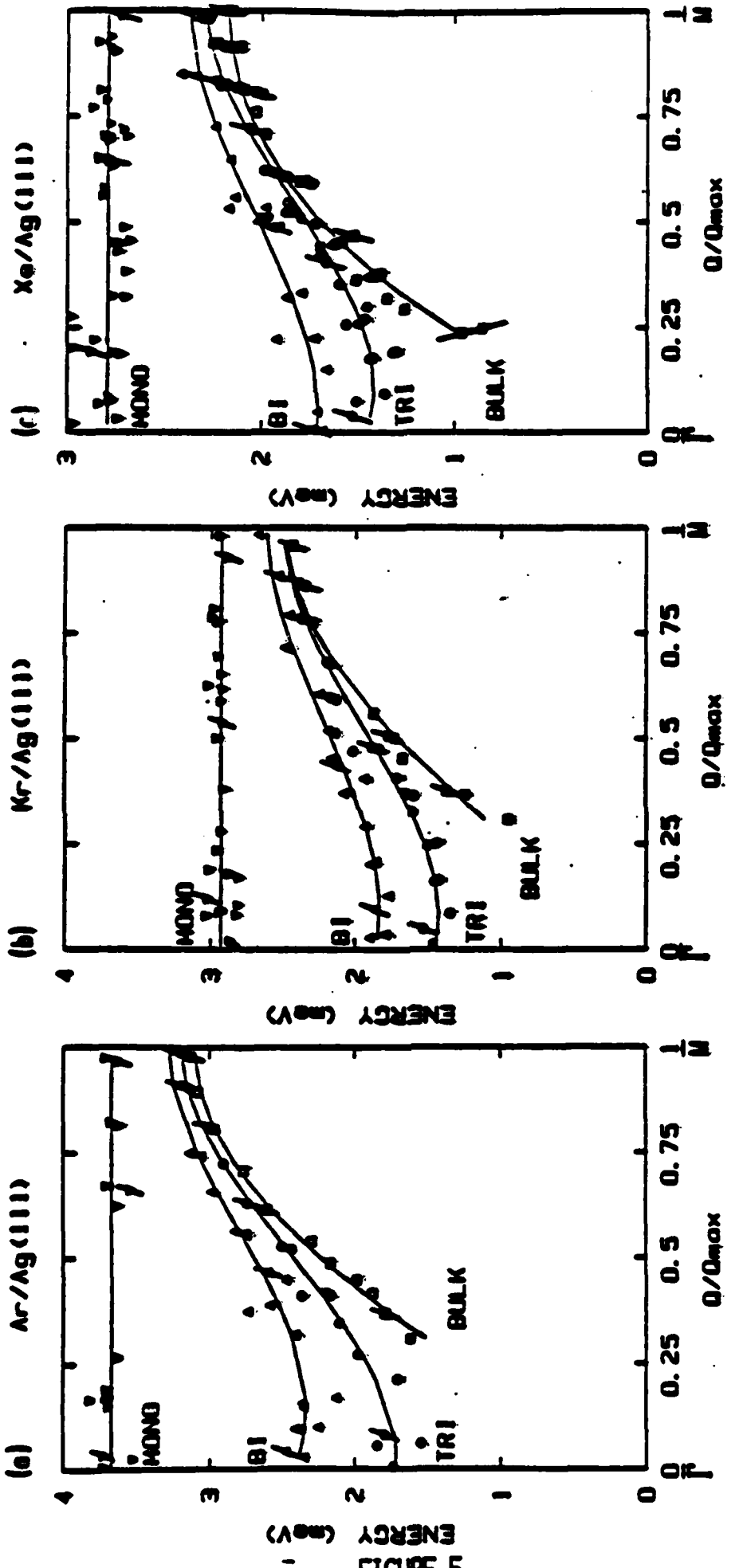
(a) Ar/Ag(111)
(b) Kr/Ag(111)
(c) Xe/Ag(111)
ENERGY (meV)
MONO
BI
TRI
BULK
0
0.25
0.5
0.75
1
Q/Qmax

FIGURE 5

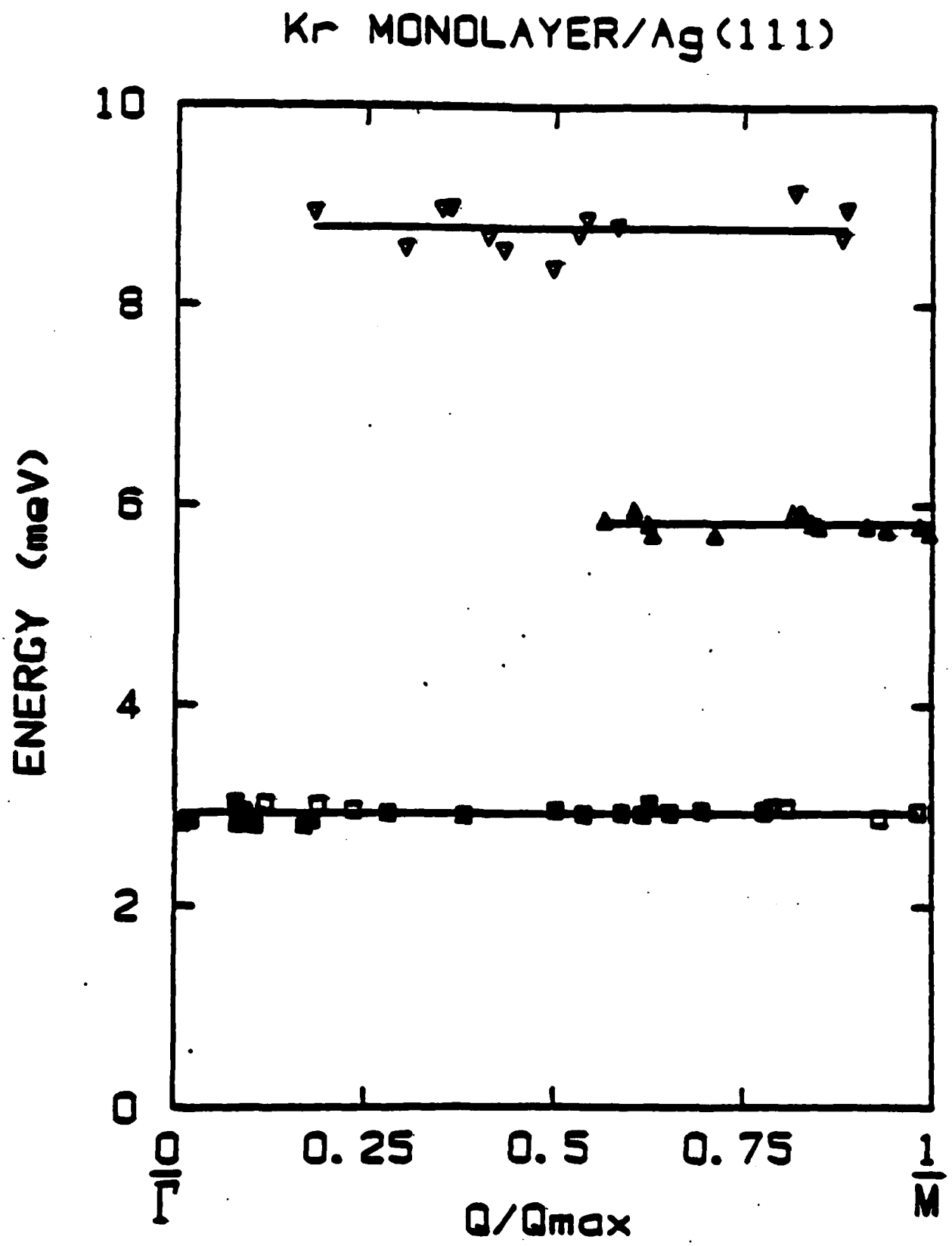

FIGURE 6

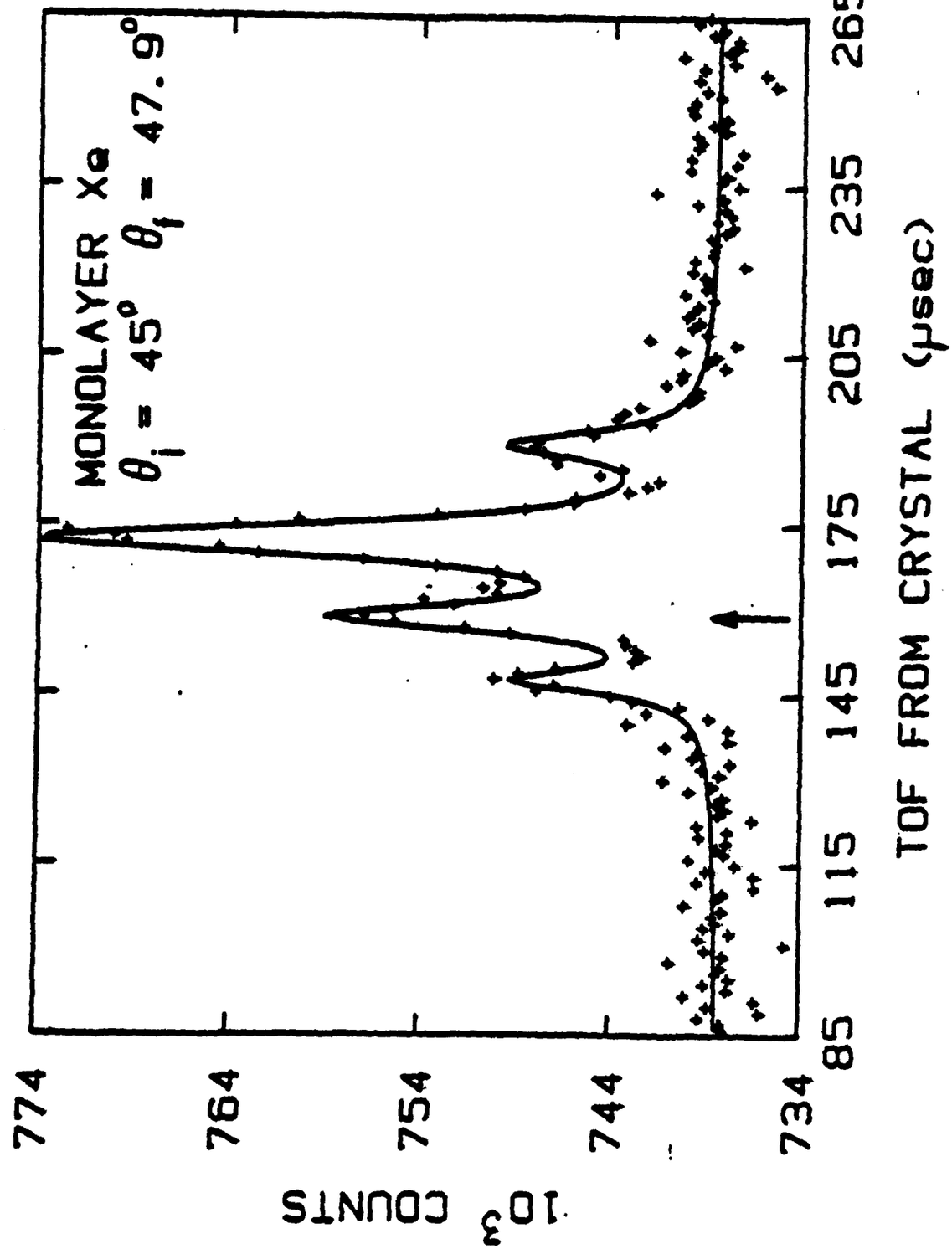
MONOLAYER Xe
$\theta_i = 45^\circ$ $\theta_f = 47.9^\circ$
774
764
754
744
734
10^3 COUNTS
85
115
145
175
205
235
265
TOF FROM CRYSTAL (μsec)

FIGURE 7

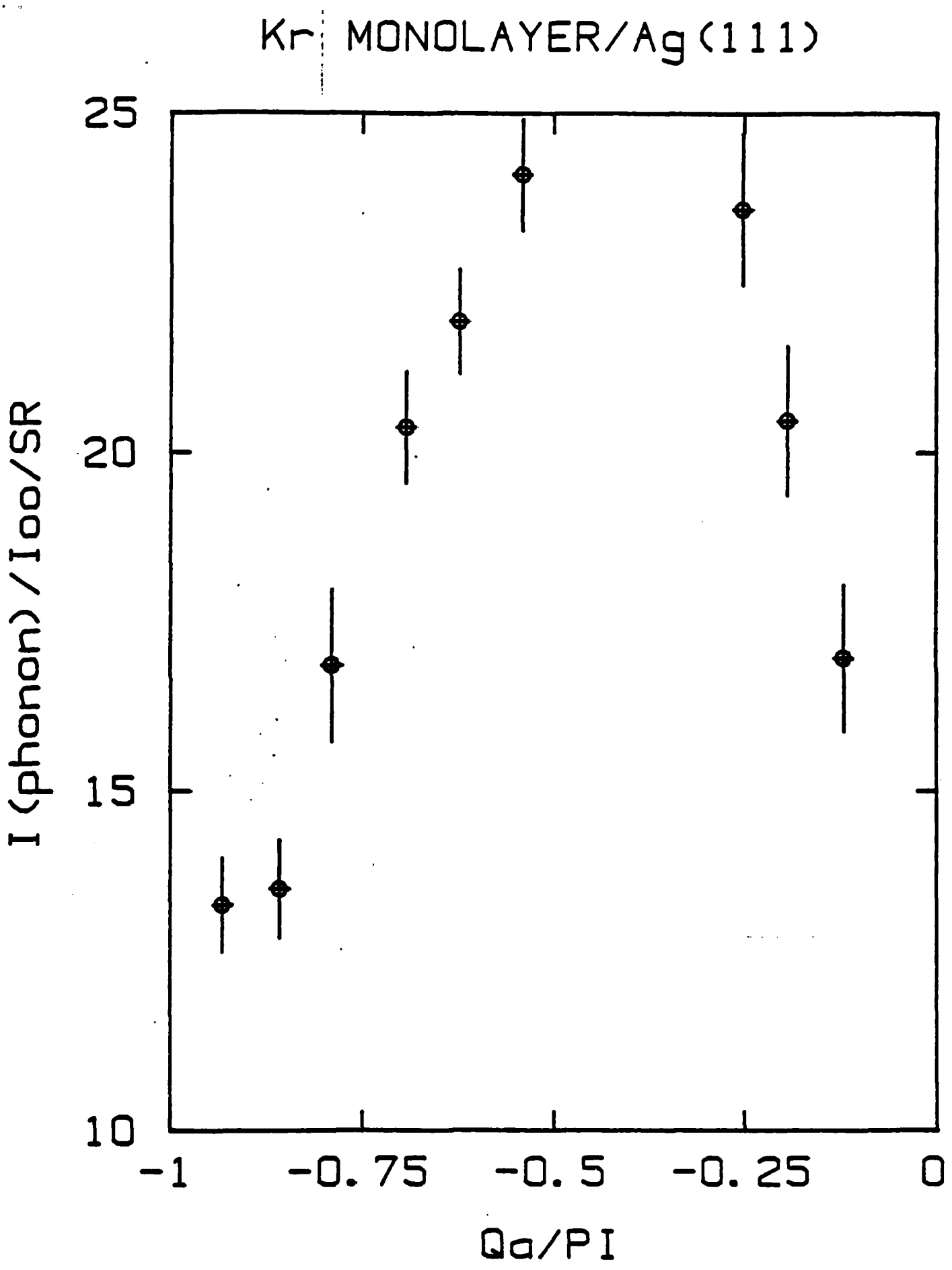
Kr MONOLAYER/Ag(111)
25
20
15
10
I(phonon)/I00/SR
-1
-0.75
-0.5
-0.25
0
Qa/PI

FIGURE 8

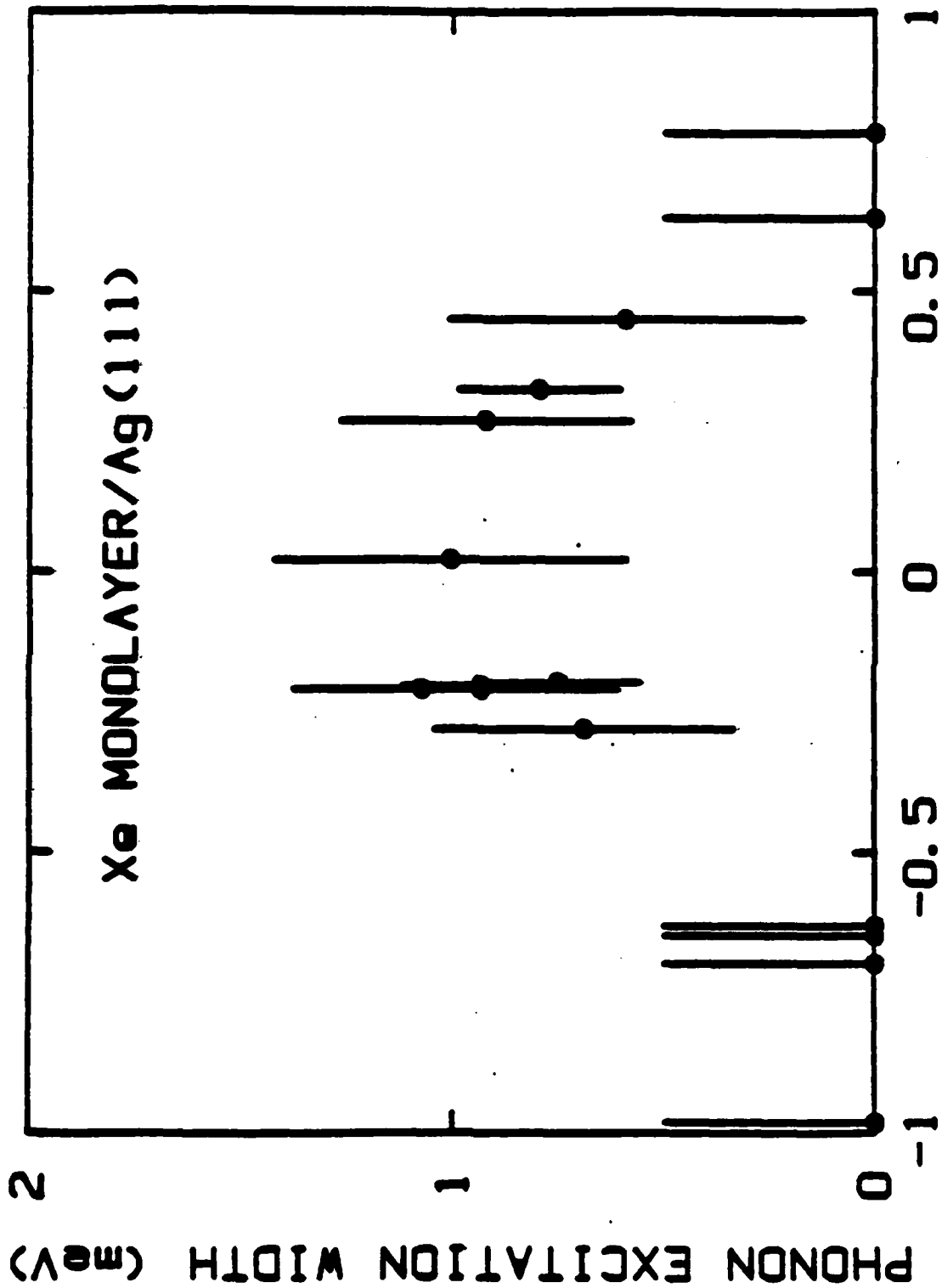
Xe MONOLAYER/Ag(111)
PHONON EXCITATION WIDTH (meV)
2
1
0
1
0.5
0
-0.5
-1
Qa/π

FIGURE 9

END

FILMED

11-85

DTIC